

The Electrode as Organolithium Reagent: Catalyst-Free Covalent Attachment of Electrochemically Active Species to an Azide-Terminated Glassy Carbon Electrode Surface

Atanu K. Das,[†] Mark H. Engelhard,[§] Fei Liu,[‡] R. Morris Bullock[†] and John A. S. Roberts^{*†}

[†] Center for Molecular Electrocatalysis, Chemical and Materials Sciences Division, P.O. Box 999, K2-57, Pacific Northwest National Laboratory, Richland, Washington 99352

[§] Environmental Molecular Sciences Laboratory, Pacific Northwest National Laboratory, Richland, Washington 99352

[‡] Department of Chemistry and School of Energy Resources, University of Wyoming, Laramie, Wyoming 82071

Supporting Information

Figures S1-S4.	S3-S6
Survey XPS spectra of glassy carbon plate samples.	
Table S1.	S7
XPS peak areas corresponding to the spectra shown in Figures S1-S4.	
Figure S5.	S7
IR spectra showing MeCN solutions of ${}^n\text{Bu}_4\text{N}^+\text{N}_3^-$ before and after addition of ICl.	
Figure S6.	S8
Reflectance IR spectra showing the glassy carbon plate substrate before and after exposure to ${}^n\text{Bu}_4\text{N}^+\text{N}_3^- + \text{ICl}$, and after subsequent exposure to $(\text{en})\text{LiC}\equiv\text{CH}$.	
Figure S7.	S8
Cyclic voltammograms of a glassy carbon electrode before and after treatment with ${}^n\text{Bu}_4\text{N}^+[\text{Cl-I-N}_3]^-$ solution, and with repeated cycling.	
Description of the baseline correction for voltammograms of surface species.	S8-S9
Figure S8.	S9
Illustration of the baseline correction.	
Figure S9.	S10-S11
Voltammograms of the samples listed in Table 2 of the main text, entries 2-6 and 8.	
Figure S10.	S12
Voltammograms showing the surface-confined ferrocenyl group obtained by reaction of $(\text{en})\text{LiC}\equiv\text{CH}$ and $\text{Fc}(\text{CH}_2)_6\text{I}$ after hand lapping in the glovebox.	
Figure S11.	S12
Voltammograms showing the surface-confined ferrocenyl group obtained by reaction of $(\text{en})\text{LiC}\equiv\text{CH}$ and $\text{Fc}(\text{CH}_2)_6\text{I}$ after mechanical lapping outside the glovebox.	
Table S2.	S13
CuAAC coupling of benzyl azide with ethynylferrocene. Conditions and yields.	
Figure S12.	S13
Cyclic voltammograms of 1-benzyl-4-ferrocenyl-1,2,3-triazole.	
Figure S13.	S14
Superimposed N 1s XPS spectra of glassy carbon samples (i) after reaction with ${}^n\text{Bu}_4\text{N}^+[\text{Cl-I-N}_3]^-$, $(\text{en})\text{LiC}\equiv\text{CH}$, and (ii) after subsequent reaction with $\text{Fc}(\text{CH}_2)_6\text{I}$.	

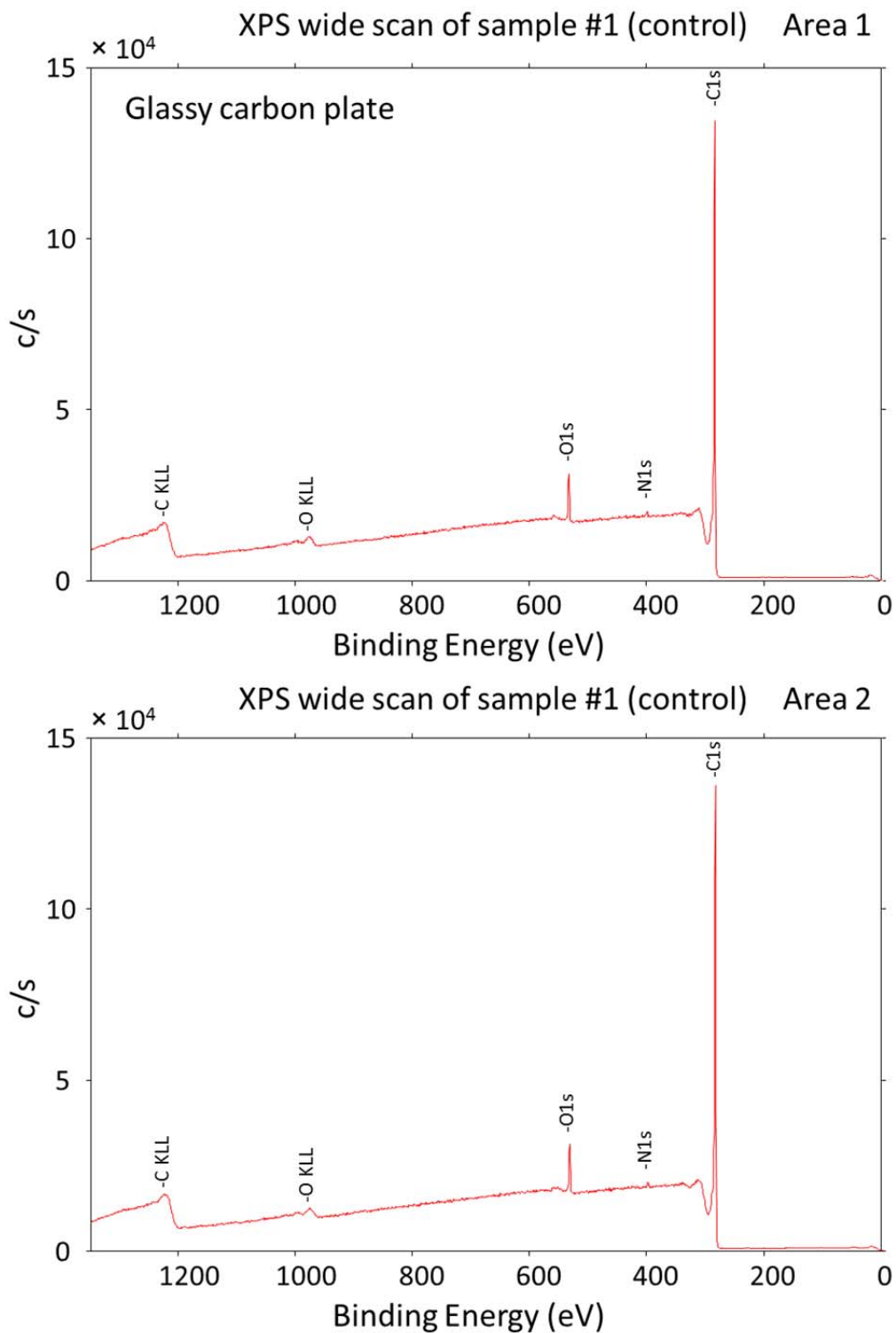


Figure S1. Survey X-Ray photoelectron spectra of a lapped + polished glassy carbon plate sample (entry 1 of Table 1).

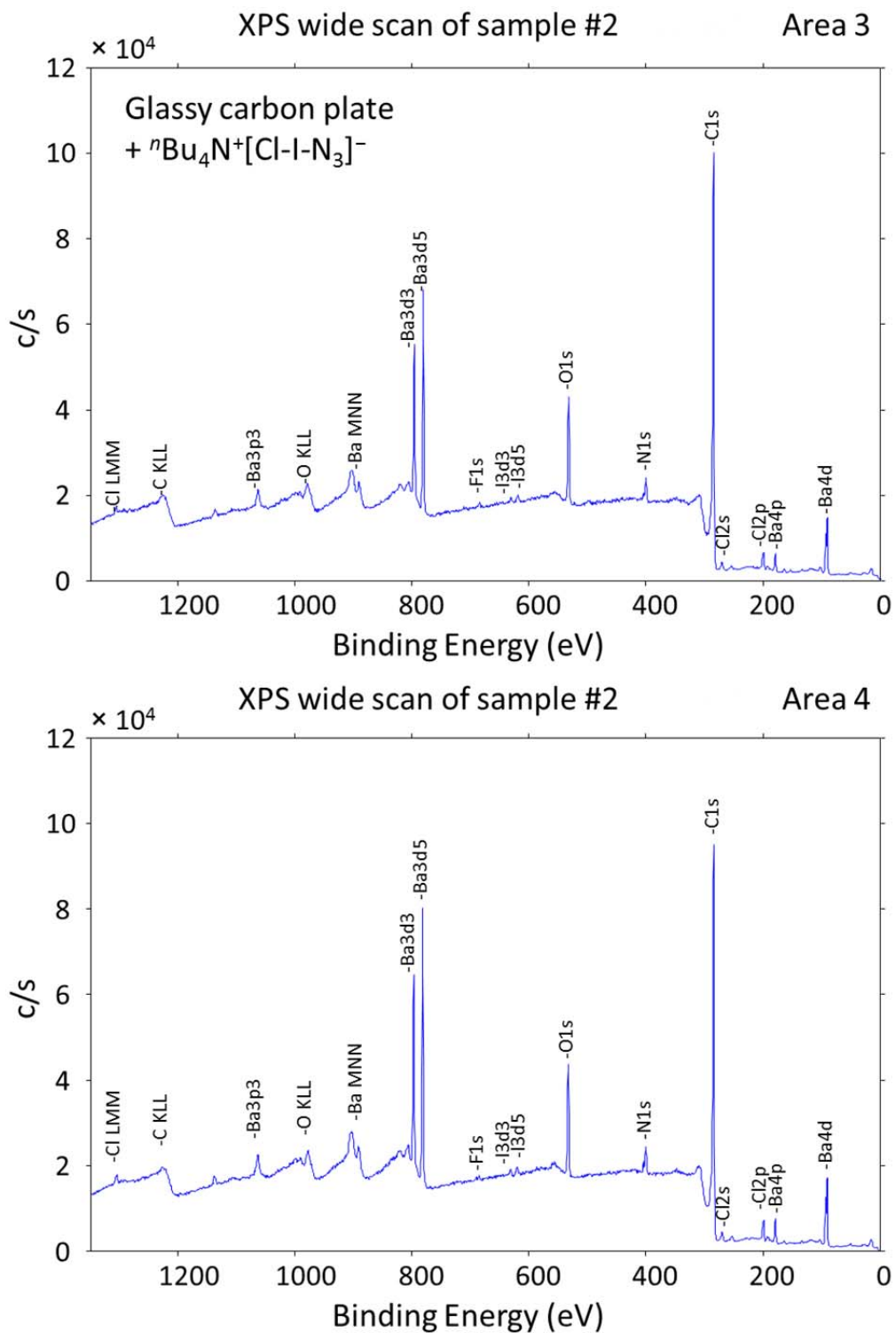


Figure S2. Survey X-Ray photoelectron spectra of a lapped + polished glassy carbon plate sample after immersion in a solution of ${}^n\text{Bu}_4\text{N}^+[\text{Cl-I-N}_3]^-$ in MeCN (entry 2 of Table 1).

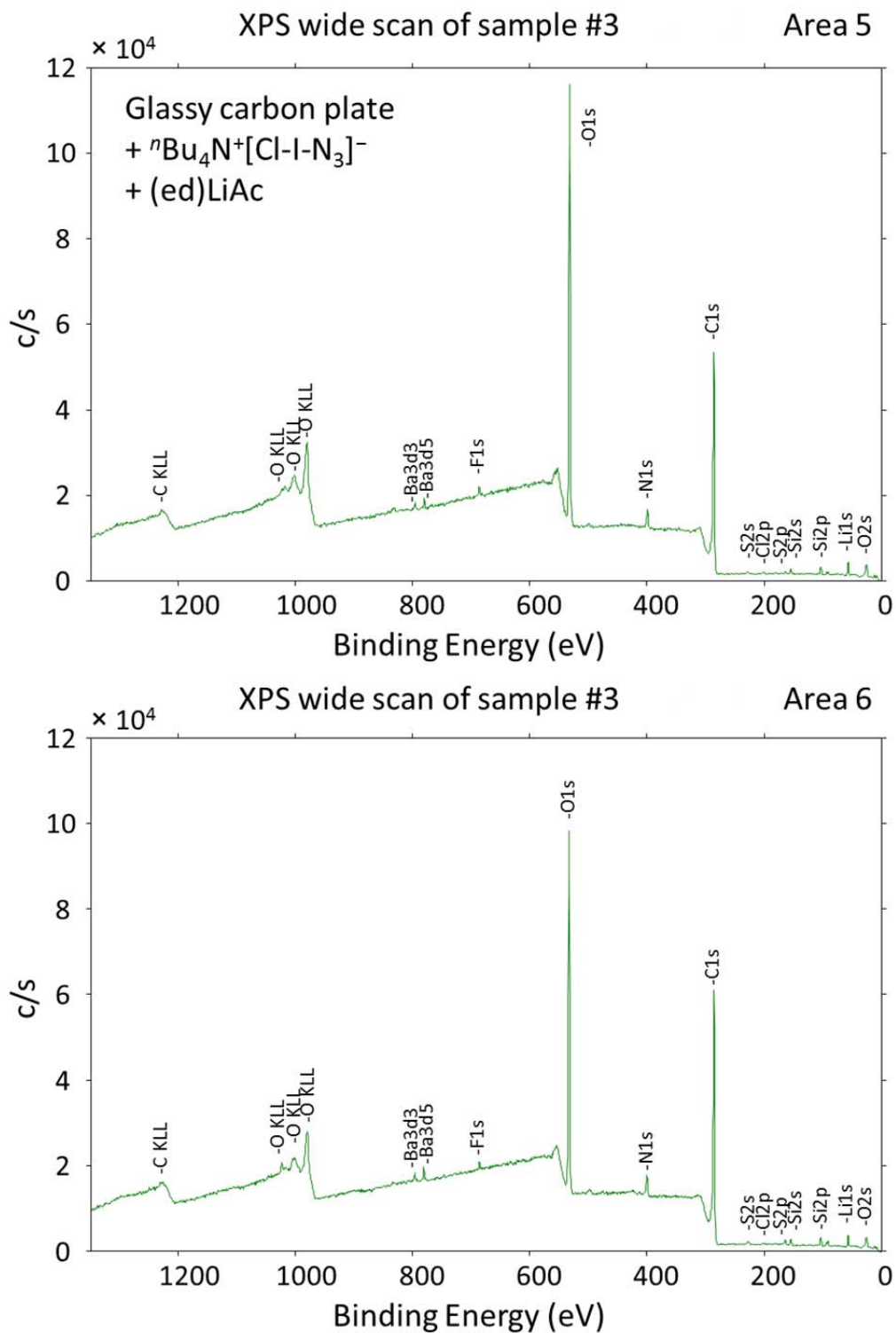


Figure S3. Survey X-Ray photoelectron spectra of a lapped + polished glassy carbon plate sample after sequential immersion in solutions of ${}^n\text{Bu}_4\text{N}^+[\text{Cl-I-N}_3]^-$ in MeCN and (en)LiC \equiv CH in THF (entry 3 of Table 1).

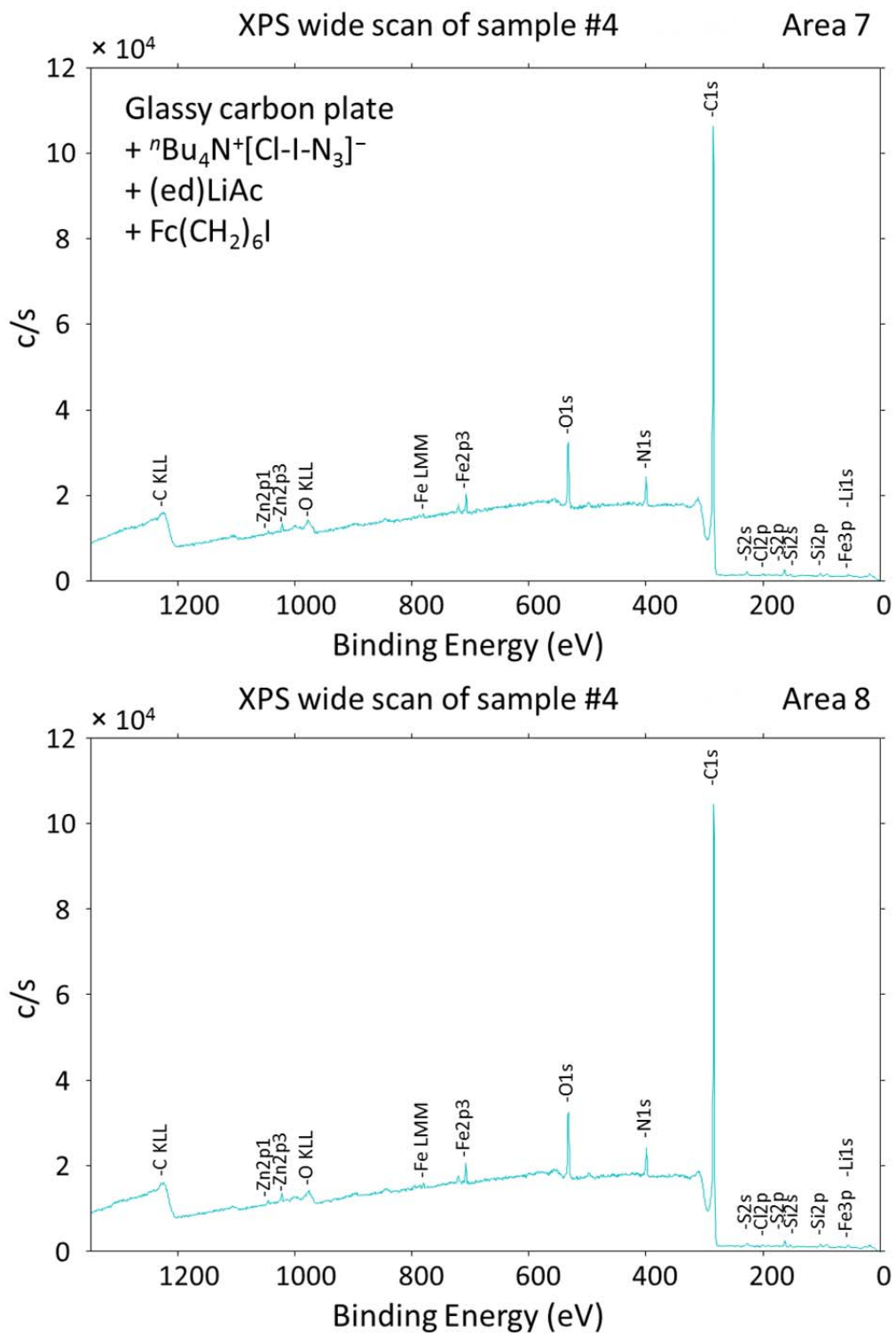


Figure S4. Survey X-Ray photoelectron spectra of a lapped + polished glassy carbon plate sample after sequential immersion in solutions of ⁿBu₄N⁺[Cl-I-N₃]⁻ in MeCN, (en)LiC≡CH in THF, and Fc(CH₂)₆I in THF (entry 4 of Table 1).

Table S1. XPS peak areas (c s^{-1}) corresponding to the spectra shown in Figures S1-S4.

		Li (1s)	C (1s)	N (1s)	O (1s)	S (2p)	Cl (2p)	Fe (2p3)	
		0.028	0.314	0.499	0.733	0.717	0.954	1.964	<i>RSF</i> ^a
sample	area	1.86	21.075	33.654	49.679	54.605	72.145	145.84	<i>Corr.</i> ^b
1	1	4	134756	1573	16399	319	99	20	
	2	0	133584	1560	15145	382	164	0	
2	1	0	108079	9892	31679	1062	5581	0	
	2	0	106465	11090	34172	941	6392	33	
3	1	3032	67976	6379	106150	781	479	0	
	2	2460	75953	6858	88143	1446	582	2.5	
4	1	455	112443	8561	17441	2120	401	3055	
	2	698	113144	8687	18632	1947	318	3713	

^a Relative sensitivity factor; see Ref. 1. ^b RSF, corrected for instrument-specific effects; see Ref. 2.

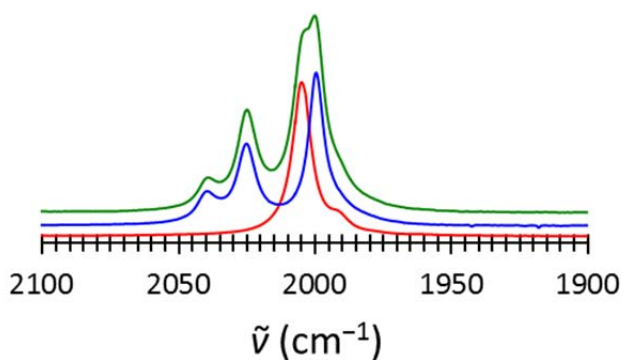


Figure S5. Background- and solvent-subtracted IR spectra showing MeCN solutions of $n\text{Bu}_4\text{N}^+\text{N}_3^-$ before (red) and after (blue) addition of ICl. The bands at 2025 cm^{-1} and 2000 cm^{-1} are also seen in the IR spectrum of the orange-red supernatant obtained on adding ICl to a NaN_3 suspension in MeCN (green). Dübigen and Dehnicke reported bands at exactly these frequencies for the halo adduct $\text{Me}_4\text{N}^+[\text{Cl-I-N}_3]^-$.³

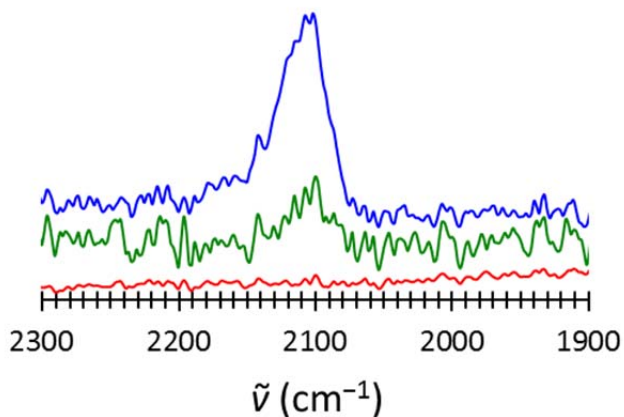


Figure S6. Background-subtracted reflectance IR spectra (45°) showing the glassy carbon plate substrate before (red) and after (blue) exposure to the mixture of ${}^n\text{Bu}_4\text{N}^+ \text{N}_3^-$ and ICl in MeCN, and after subsequent exposure to (en)LiC≡CH in THF (green).

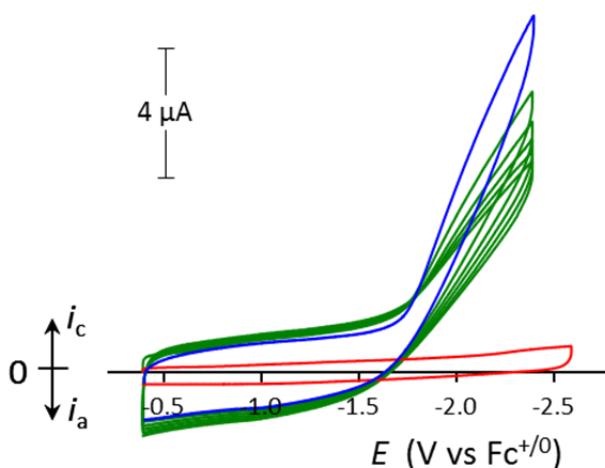


Figure S7. Cyclic voltammogram of a glassy carbon electrode in MeCN ($0.1 \text{ M } {}^n\text{Bu}_4\text{N}^+\text{PF}_6^-$, $\nu = 0.1 \text{ V s}^{-1}$) before (red) and after (blue) treatment with ${}^n\text{Bu}_4\text{N}^+[\text{Cl-I-N}_3]^-$ solution. Decay in the Faradaic current on repeated scanning (green).

Baseline Correction. The data were smoothed using the rolling average method, with each set of p consecutive points averaged to give the new value of the middle point in that set. For this study, $p = 11$. The smoothed data was used only to estimate the slope m_{pf} of the current function $i(E)$ at the peak foot potentials E_{pf} according to eq. S1.

$$m_{\text{pf}} = \left. \frac{di(E)}{dE} \right|_{E_{\text{pf}}} \cong \frac{\sum_{x=1}^n i_{\text{s}}(E_{\text{pf}} - x\Delta E) - i_{\text{s}}(E_{\text{pf}} + x\Delta E)}{2 \sum_{x=1}^n x} \quad (\text{S1})$$

where ΔE is the potential increment, $i_s(E)$ is the smoothed current function, and n is the number of potential increments over which the sum was computed; in the present case, $n = 10$.

The slopes at each peak foot potential were used to construct two functions $i_{pf,+}(E)$ and $i_{pf,-}(E)$ with $i_{pf,+}(E)$ passing through the positive peak foot and $i_{pf,-}(E)$ passing through the negative peak foot, and with slopes evolving according to eq. S2. (blue traces, Figure S8 below).

$$\frac{\Delta i_{pf,+}(E)}{\Delta E} = \frac{\Delta i_{pf,-}(E)}{\Delta E} = \frac{(E - E_{pf,-})m_{pf,+} + (E_{pf,+} - E)m_{pf,-}}{E_{pf,+} - E_{pf,-}} \quad (\text{S2})$$

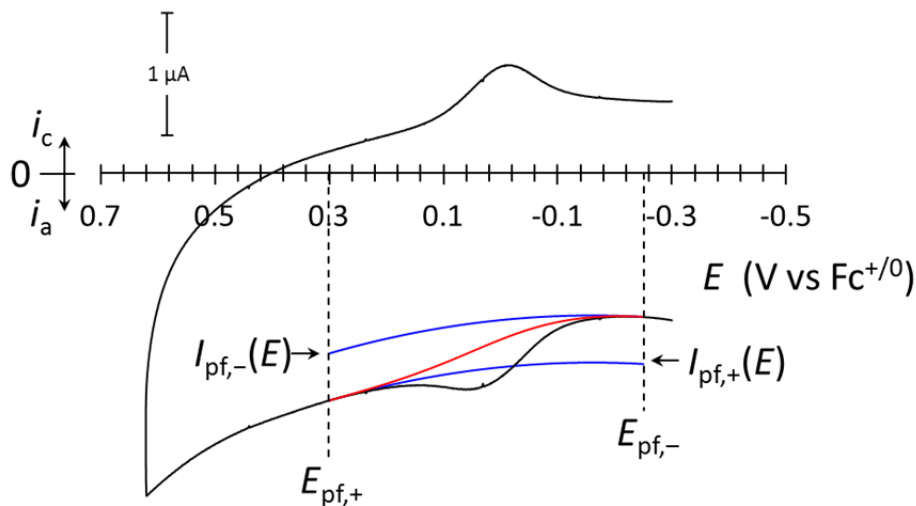


Figure S8. Construction of the baseline function $i_b(E)$ (red) from the peak foot functions $i_{pf,+}(E)$ and $i_{pf,-}(E)$ (blue). Original CV trace is shown in black.

The baseline function $i_b(E)$ was constructed (red trace, Figure S8) from $i_{pf,+}(E)$ and $i_{pf,-}(E)$ according to eq. 3 with the manually adjusted weighting parameter w ranging from 1 to 2.

$$i_b(E) = \frac{(E - E_{pf,-})^w i_{pf,+}(E) + (E_{pf,+} - E)^w i_{pf,-}(E)}{(E - E_{pf,-})^w + (E_{pf,+} - E)^w} \quad (\text{S3})$$

Varying w changes the sharpness of the curvature of $i_b(E)$ and affects the formula widths at half-maximum height (FWHM values) of the baseline-corrected data but does not affect the total charge passed and thus does not influence coverages calculated by integrating the baseline-subtracted waves.

This baseline correction strategy was developed for surface confined species. It is possible to adjust the inputs $E_{pf,+}$, $E_{pf,-}$, and w to obtain fairly symmetrical “baseline subtracted” waves even from diffusive waves. For this reason, data prepared in this way is not suitable for demonstrating surface attachment; this is best done by examining peak current-scan rate dependence and peak-to-peak separations, augmented by practical controls such as thorough rinsing and transfer to fresh electrolyte and by surface analyses such as XPS.

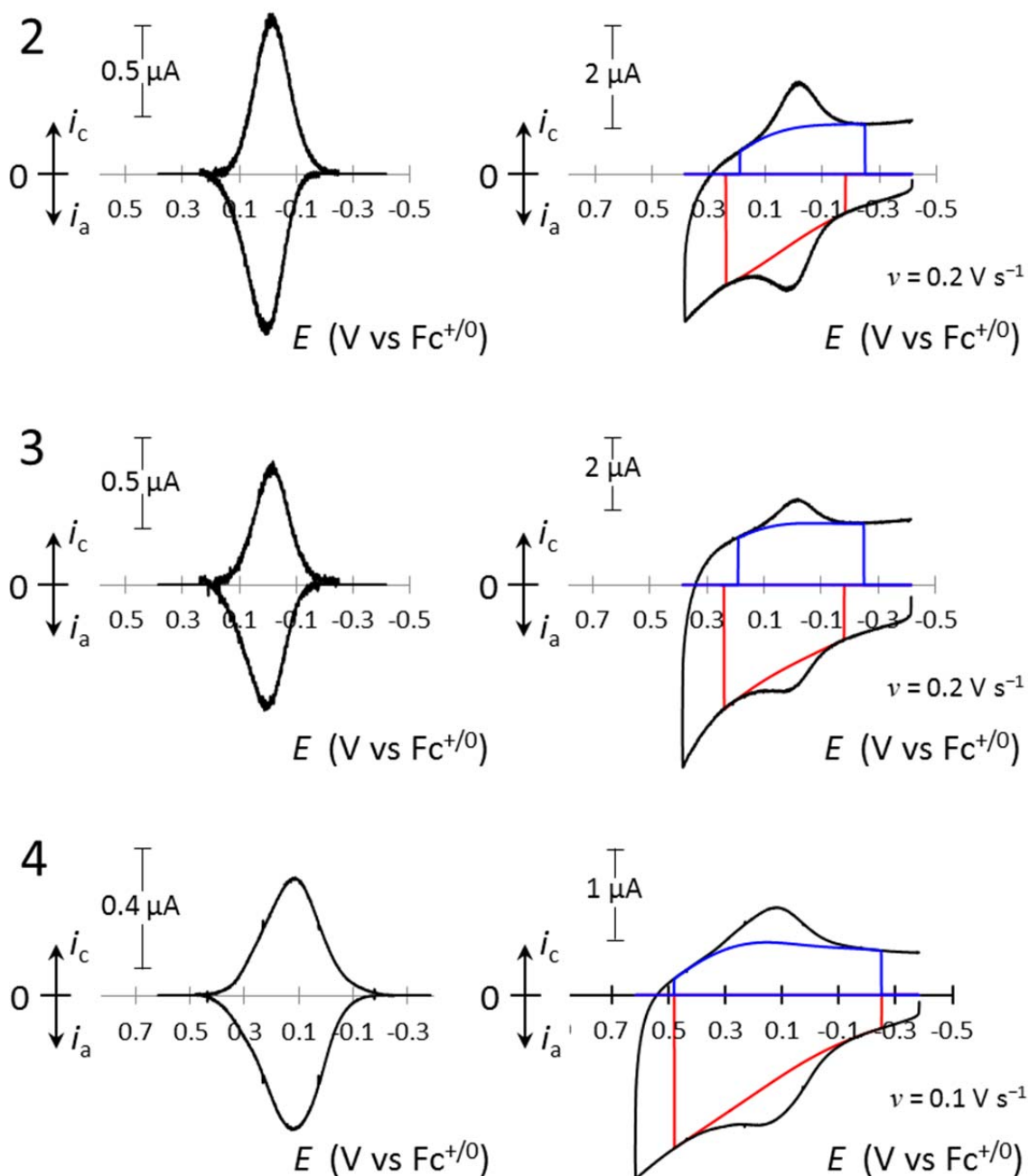


Figure S9 (part 1 of 2). Baseline-corrected voltammograms (raw data at right) of the samples listed in Table 2 of the main text. Interpolated baselines are shown in red and blue. MeCN (0.1 M $n\text{Bu}_4\text{N}^+\text{PF}_6^-$). Voltammograms corresponding to entries 1 and 6 appear in the text (figures 2 and 4, respectively).

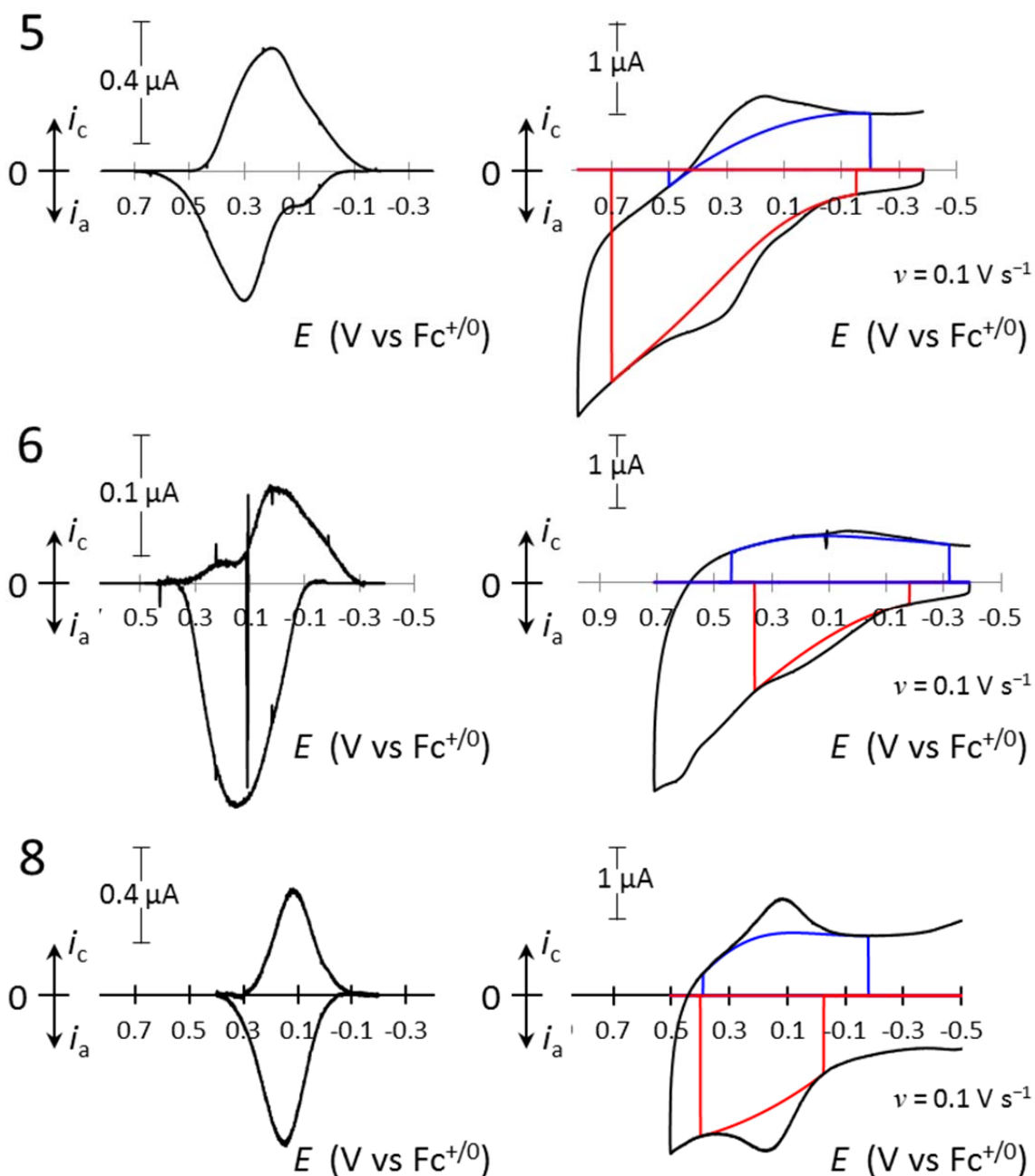


Figure S9 (part 2 of 2). Baseline-corrected voltammograms (raw data at right) of the samples listed in Table 2 of the main text. Interpolated baselines are shown in red and blue. MeCN (0.1 M $n\text{Bu}_4\text{N}^+\text{PF}_6^-$). Voltammograms corresponding to entries 1 and 6 appear in the text (figures 2 and 4, respectively).

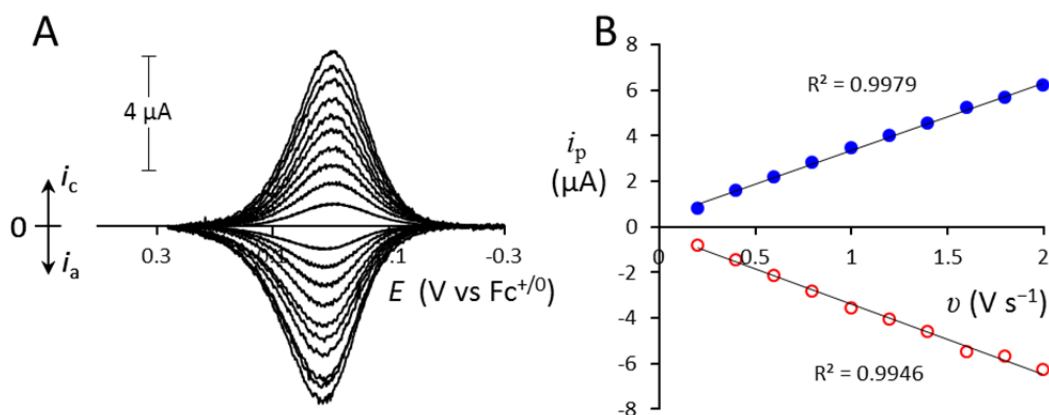


Figure S10. (A) Baseline-corrected voltammograms collected at different scan rates in MeCN ($0.1 \text{ M } ^n\text{Bu}_4\text{N}^+\text{PF}_6^-$) corresponding to entry 2 of Table 2 in the main text. (B) Dependence of the corresponding cathodic and anodic peak currents on the scan rate v ($0.1\text{-}2 \text{ V s}^{-1}$).

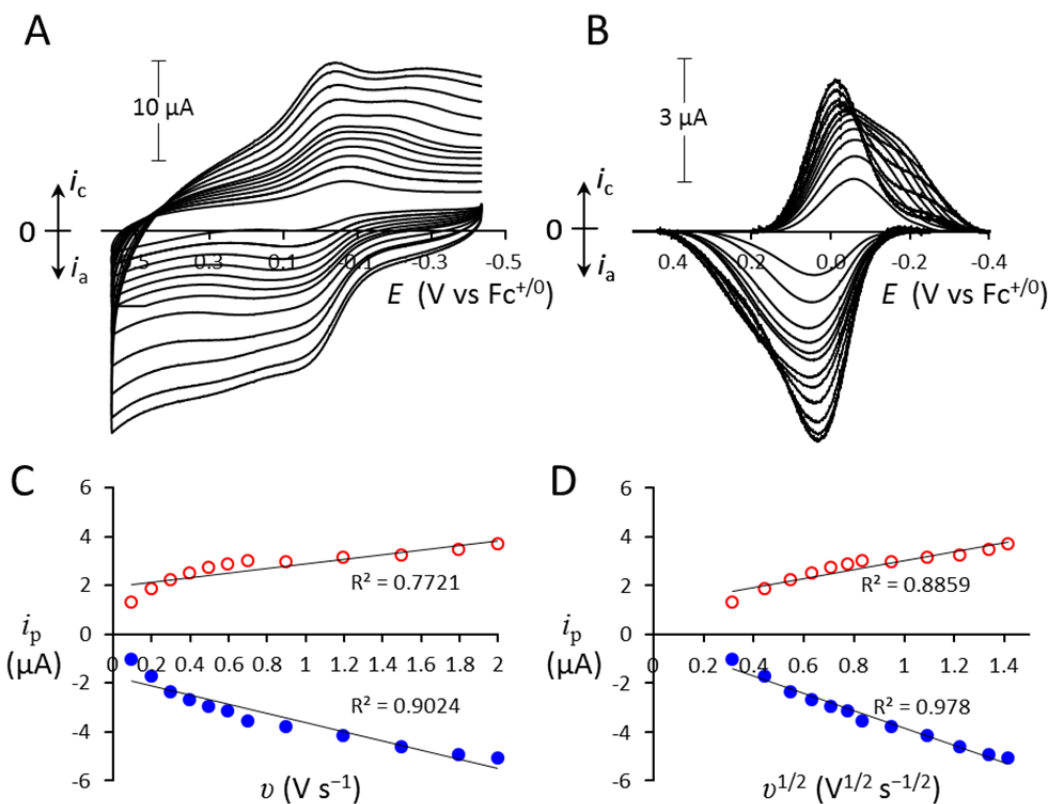


Figure S11. Raw (A) and baseline-corrected (B) voltammograms collected at different scan rates in MeCN ($0.1 \text{ M } ^n\text{Bu}_4\text{N}^+\text{PF}_6^-$), showing the surface-confined ferrocenyl group obtained by mechanical lapping outside the glovebox and polishing inside the glovebox, followed by sonication and stirring with activated carbon in EtOH and sequential immersion in solutions of $^n\text{Bu}_4\text{N}^+[\text{Cl-I-N}_3]^-$ in MeCN, (en)LiC \equiv CH in THF, and $\text{Fc}(\text{CH}_2)_6\text{I}$ in THF. Linear fits to the peak currents vs scan rate v (C) and vs $v^{1/2}$ (D).

Table S2. CuAAC Coupling of Benzyl Azide with Ethynylferrocene. Conditions and Spectroscopic Yields

Entry	Cu catalyst	Base	Time	Solvent	Yield ^a
1	Cu(CH ₃ CN) ₄ PF ₆	–	24 h	THF	0%
2	Cu(CH ₃ CN) ₄ PF ₆	<i>i</i> Pr ₂ EtN	24 h	THF	58%
3	Cu(CH ₃ CN) ₄ PF ₆	<i>i</i> Pr ₂ EtN	24 h	9:1 DCM:MeOH	20%
4	Cu(CH ₃ CN) ₄ PF ₆	<i>i</i> Pr ₂ EtN	50 h	9:1 DCM:MeOH	30%
5	Cu(CH ₃ CN) ₄ PF ₆	Et ₃ N	24 h	THF	75%
6	Cu(CH ₃ CN) ₄ PF ₆	Et ₃ N	24 h	MeCN	80%
7	CuI	<i>i</i> Pr ₂ EtN	24 h	THF	62%
8	CuI	<i>i</i> Pr ₂ EtN ^b	24 h	THF	56%
9	CuI	Et ₃ N	24 h	THF	82%
10	CuSO ₄ + sodium ascorbate	–	24 h	1:1 DMSO:Water	85%

^a Calculated based on comparing the absorbance before and after the reaction. ^b Hydroquinone added as reductant.

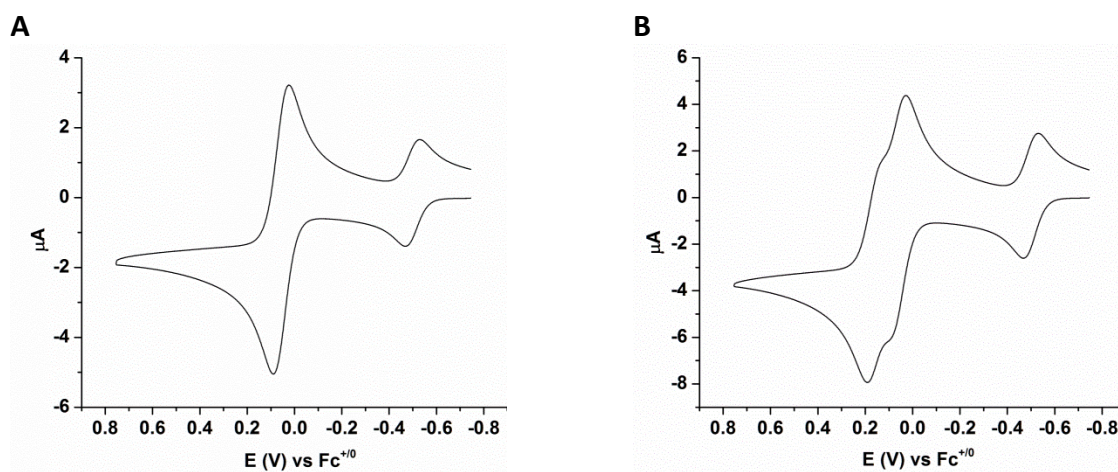


Figure S12. Cyclic voltammograms of 1-benzyl-4-ferrocenyl-1,2,3-triazole in MeCN (0.1 M $n\text{-Bu}_4\text{N}^+\text{PF}_6^-$ with permethylferrocene as internal standard, $\nu = 0.1 \text{ V s}^{-1}$) both without (A) and with (B) added ethynylferrocene.

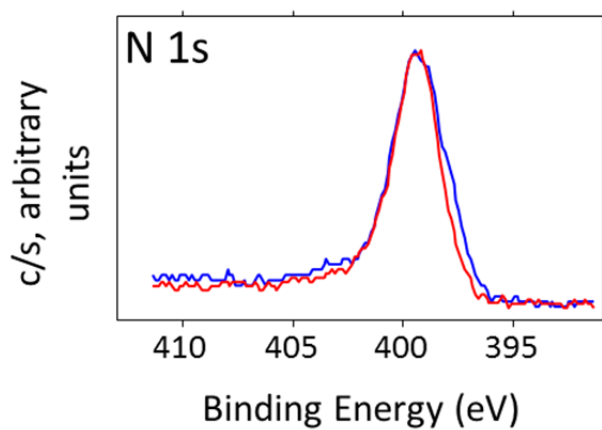


Figure S13. Normalized, superimposed high-resolution photoemission spectra (N 1s photoelectron region) of glassy carbon plate samples after reaction with $n\text{Bu}_4\text{N}^+[\text{Cl-I-N}_3]^-$ and (en)LiC \equiv CH (blue trace), and after subsequent reaction with Fc(CH $_2$) $_6$ I (red trace).

References

1. Wagner, C. D.; Davis, L. E.; Zeller, M. V.; Taylor, J. A.; Raymond, R. H.; Gale, L. H. *Surf. Interface Anal.* **1981**, *3*, 211-225.
2. Powell, C. J.; Seah, M. P. *J. Vac. Sci. Technol., A* **1990**, *8*, 735-763.
3. Dübgen, R.; Dehnicke, K. *Naturwissenschaften* **1978**, *65*, 535-535.